



# Single-step deposition of hexamethyldisiloxane surface gradient coatings with a high amplitude of water contact angles over a polyethylene foil

Hediyeh Malekzad<sup>1,2</sup>  | Tommaso Gallingani<sup>3</sup> | Federica Barletta<sup>3</sup>  |  
Matteo Gherardi<sup>3,4</sup> | Vittorio Colombo<sup>3,4</sup> | David Duday<sup>1</sup>

<sup>1</sup>Materials Research and Technology, Luxembourg Institute of Science and Technology, Belvaux, Luxembourg

<sup>2</sup>Doctoral School in Science and Engineering (DSSE), Faculty of Science, Technology and Medicine (FSTM), University of Luxembourg, Belval, Luxembourg

<sup>3</sup>Department of Industrial Engineering (DIN), Alma Mater Studiorum—Università di Bologna, Bologna, Italy

<sup>4</sup>Interdepartmental Centre for Industrial Research in Advanced Mechanical Engineering Applications and Materials Technology, Università di Bologna, Bologna, Italy

## Correspondence

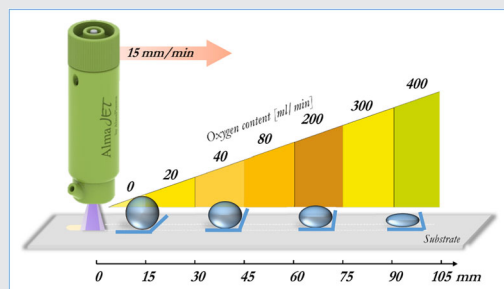
David Duday, Materials Research and Technology, Luxembourg Institute of Science and Technology, 41 rue du Brill, Belvaux 4422, Luxembourg.  
Email: david.duday@list.lu

## Funding information

Fonds National de la Recherche Luxembourg, Grant/Award Number: FNR PRIDE/15/10935404.

## Abstract

One interesting category of nano- and micro-engineered surfaces is surface gradients, which allow the controlled optimization of biointerfaces at a small scale in an extended area length. Plasma coatings offer a large diversity of functionalities at the nanoscale, accompanied by high chemical stability and adhesion on a variety of substrates at ambient temperature. Atmospheric-pressure plasma-assisted deposition could be employed the generation of surface gradients on thermosensitive materials. In this study, a corona plasma jet is used to deposit polydimethylsiloxane/SiO<sub>2</sub>-like surface gradients on polyethylene foil by varying the O<sub>2</sub> concentration in the discharge during the movement of the plasma source. We obtained, in a single-step approach, gradient coatings along a length of ~10 cm, with a gradual variation of both chemistry and surface energy.



## KEYWORDS

chemistry gradient, hexamethyldisiloxane, plasma jet, plasma-enhanced chemical vapor deposition, water contact angle

## 1 | INTRODUCTION

It is already known that some functional groups, such as amines, CH<sub>x</sub>, CF<sub>x</sub>, or carboxylic acid groups can favor protein adsorption. Hence, surfaces modified with these functionalities can be used for tissue regeneration,

biosensors, drug release systems, and so forth. However, ether, hydroxyl, and thiol groups decrease biofouling processes and can be employed in the marine industry or for antimicrobial applications.<sup>[1,2]</sup> The optimization of such functional surfaces for devices in contact with complex biological media is generally complex and long. Therefore,

This is an open access article under the terms of the Creative Commons Attribution-NonCommercial-NoDerivs License, which permits use and distribution in any medium, provided the original work is properly cited, the use is non-commercial and no modifications or adaptations are made.

© 2020 The Authors. *Plasma Processes and Polymers* published by Wiley-VCH GmbH

any approaches, such as surface gradients, which allow the faster development of these surfaces, are welcome by biomedical device developers and manufacturers.

A surface gradient enables a systematic study of the impact of gradually varying experimental parameters by conducting a single experiment, using a single surface and keeping experimental conditions identical.<sup>[3]</sup> Therefore, this method is highly preferential for developing high-performance biosensing platforms or devices for cell guiding or sorting. These advantages will guarantee high reproducibility or high throughput along with considerable time and cost savings. Nevertheless, to fully benefit from the advantages of surface gradients, the ideal method is to develop gradients under less-complicated operational systems to create the possibility of upscaling with a linear change of a variable over a large range of distances for a better prediction of correlation between chemical/topographical/mechanical cues and biological events.

After developing the gradient of the desired property over the surface, the gradual change in the variable is correlated to the length of the gradient. Later, the region with the highest adsorption, proliferation, differentiation, or any other biological event will be selected and validated by testing the generated gradient in the presence of the desired bioreaction and targeted physiological conditions. For the example of biosensors, the area with optimal adsorption, corresponding to optimal density and biomolecular orientation, is expected to be used as the reference surface for biosensor development. In the case of biosensors, the bioreaction is typically the recognition of the labeled biomolecule with its complementary molecule (antibody, enzyme, etc.), the receptor, which is already immobilized over the surface. The receptor density is expected to be higher in a region with a gradient with specific properties, giving rise to the highest detectable signal.<sup>[4]</sup> Another possible biosensing scheme is detecting the response of cells toward areas with desired wettability and mechanical and topographic properties of the gradient, which they choose to proliferate, differentiate, and so forth, and which can be recognized by detecting the relevant biomarkers or imaging techniques.<sup>[5]</sup>

The applications of the surface gradients are not limited to exploring the high-performance area but can also be used as a driving tool for initiating biological phenomena such as cell migration (e.g., bacterial chemotaxis).<sup>[6]</sup> One important implication of cell motility is cell response to the chemoattractant gradient, which is the cause of important health issues such as metastasis of cancerous cells,<sup>[7]</sup> for instance, the role of the fetal bovine serum gradient in metastatic breast cancer cells and the degree of chemotaxis.<sup>[8]</sup>

Several techniques have already been used to generate surface gradients, such as self-assembled monolayer, dipping, spin coating, and so forth. However, not all of these techniques allow us to simultaneously control the surface characteristics at the nano-, micro-, and macroscales, and not all simultaneously provide high throughput and high flexibility. Plasma polymerization techniques can offer these advantages. Here, reactions take place in the gas phase and are eco-friendly, providing a high density of the desired functional groups,<sup>[9]</sup> and most important, they enable surfaces to be coated, regardless of the substrate type. Also, taking advantage of the atmospheric nonequilibrium pressure plasmas, it is possible to coat thermosensitive substrates, owing to a moderate discharge temperature ( $T \sim 40^\circ\text{C}$ ) and the atmospheric pressure operational conditions of cold plasmas.

Controlling plasma parameters, it is possible to tailor the mechanical and chemical stability of the polymer coatings independently,<sup>[10]</sup> which is not straightforward with other techniques, because it requires structural changes to be applied during the synthesis of polymers.<sup>[11]</sup> There are two possible ways of generating surface gradients by plasma: one is based on passing a reactive gas over a surface and activating functional groups of the substrate, and the other is based on the deposition and polymerization of the precursor over a substrate. There are few reports on using plasma polymerization for the generation of chemistry or wettability gradients by deposition techniques.<sup>[5,12–16]</sup> However, some of the plasma-generated gradient studies reported so far are based on the activation of the surface in the absence of a precursor, solely by passing varying amounts of  $\text{O}_2$  over it,<sup>[17–22]</sup> which generally leads to non-durable surface properties.

The plasma polymer concentration gradient can be implemented by tuning the flow rate of a precursor, the ratio of flow rates (in the case of two precursors), and/or by changing the plasma power input to achieve a different degree of precursor fragmentation, leading to a variation in the deposited film. This composition change should be accompanied either by spatial displacement of the sample in regard to the plasma source or by using a mask.

The majority of the reported plasma polymer gradients in the literature focus on introducing amino-functional groups at one end of the coating and methyl-rich groups at the other end by changing the flow rate ratio of the two relevant precursors. The varying precursor composition is introduced as follows: either the sample placed inside the plasma chamber (in vacuum plasmas) is masked/exposed or the plasma needle is gradually displaced along the sample (atmospheric-pressure plasmas); besides, a varying ratio of the two precursors (or ratio of one precursor and one gas) is

delivered by the plasma itself.<sup>[23]</sup> Frequently reported precursors for generating plasma polymers are carboxylic acid and/or amino-functional acrylic acid, and allylamine along with apolar hydrocarbon precursors such as 1,7-octadiene (OD), and the gradients generated are used mainly for cell studies.<sup>[24–26]</sup> In another study, the thickness gradient of glycol dimethyl ether was generated on top of the acrylic acid plasma polymer platform by using a tilted mask. The results proved that the cell attachment and morphology varied as a function of the surface chemistry gradient.<sup>[14]</sup> Similar studies have been conducted using plasma polymerization with OD and acrylic acid as a gradient generating species based on a moving mask to form nonpolar functional groups on one side and negatively charged species on the other side. The characterization of the sample surface after the covalent coupling of the antibodies and the later application of fluorescent-linked ligand have demonstrated an antibody activity gradient along with the coating.<sup>[27]</sup>

Klages et al., have generated a plasma coating chemical gradient with organosilicon, hexane-1-ol, and glycidyl methacrylate precursors in a single-step mode and without a mask.<sup>[28]</sup> However, this approach is not flexible (one reactor needed for one specific gradient), and currently, it does not seem adequate for generating functional gradients, because it is also very difficult to upscale. It is an approach for more fundamental research.

The plasma approach reported in this study is maskless (plasma jet), flexible, upscalable, and combines an automated movement procedure with the deposition of the precursor for the generation of durable plasma polymer coatings with wettability and chemistry gradients, and as it is a one-step simple approach, it has advantages over previously reported similar plasma-generated chemical gradient approaches.

We report here on the generation of corona plasma jet-deposited surface chemistry and wettability gradients by using hexamethyldisiloxane (HMDSO) as a precursor and by continuously varying the O<sub>2</sub> flow rate. We show here that it is possible to generate such a gradient with a continuous increase of inorganic character and wettability at the 10-cm scale on a thermally sensitive polymer foil.

## 2 | EXPERIMENTAL

### 2.1 | Plasma-assisted deposition

#### 2.1.1 | AlmaPLUS plasma setup

All the experiments were performed using a fully automated system (AlmaPLUS; AlmaPlasma s.r.l.) equipped with a CNC pantograph and a remotely controlled high-

voltage pulsed generator (AlmaPULSE, AlmaPlasma s.r.l.). The system also includes a remotely controlled liquid and gas console composed of four mass flow controllers (EL-FLOW; Bronkhorst), a liquid flow meter (miniCORI flow; Bronkhorst) and a controlled evaporation mixer (Bronkhorst). The plasma source, fixed on the head of the CNC system, is a single high-voltage electrode corona jet (AlmaJET), as described in Reference [29], which is well suited for localized plasma treatments and the deposition of complex three-dimensional coatings. In the plasma polymerization experiments reported in this paper, the primary gas introduced into the plasma discharge region from the upper part of the source consisted of 2.0 slpm of argon (Ar) and 0.2 g/hr (0.0043 ml/min) of HMDSO (Sigma-Aldrich). Different oxygen values range from 0 to 400 ml/min (0–0.4 slpm), which can also be defined either as percentages with respect to the whole carrier gas inside the plasma O<sub>2</sub>/(O<sub>2</sub> + Ar; 0–7.4%) or molar ratios of it with respect to the fixed precursor rate (O<sub>2</sub>/HMDSO): 0, 17, 35, 70, 175, 262, 350, which are added to generate the gradients.

A secondary gas (3 slpm of Ar) was injected through a diffuser in the region downstream of the high-voltage electrode tip. A shroud gas (3 slpm of nitrogen, N<sub>2</sub>) was also injected at the outlet of the plasma source using a further gas diffuser, specifically designed to confine the plasma discharge from the surrounding environment. The distances between the tip of the plasma jet and the substrate were kept constant at 15 mm. The deposition of circular coatings or spots (“static mode”) and gradient (“dynamic mode”) samples was performed on polyethylene (PE) films (thickness: 500 μm). The size of the spots was ~2 cm with a deposition time of 60 s, and the gradient coating was deposited at a speed of 15 mm/min.

The AlmaJet setup including inlets and the generated filamentary plasma are shown in Figure 1.

#### 2.1.2 | Static and linear deposition

Single spots (“static mode”) of HMDSO polymers were deposited on PE transparent films with 60-s treatment time. In total, seven samples were prepared using static deposition, starting from the first sample without oxygen, and gradually increasing the O<sub>2</sub> content up to 400 ml/min, that is, 7.4% O<sub>2</sub> content.

After optimization of the parameters for static deposition, similar parameters were translated to the dynamic deposition with a 15-mm/min process speed (i.e., moving speed of the plasma jet). The oxygen flow rate started from 0 to 80 ml/min O<sub>2</sub> (0–1.6%), and electrical parameters were kept constant at 12 kV–12 kHz. However, above 80 ml/min (3.8%), the electrical conditions were increased to 15 kV–15 kHz to provide more power for sufficient gas

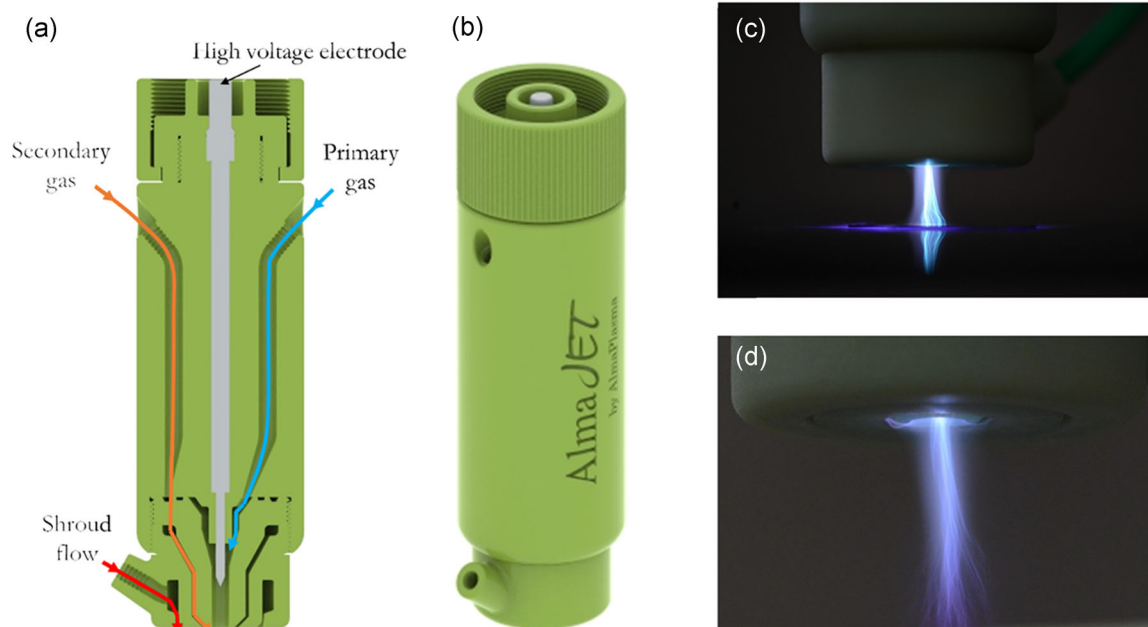


**FIGURE 1** AlmaJET plasma source. (a) Details of gas injection channels; (b) three-dimensional rendering of AlmaJET; (c) plasma treatment of a substrate; (d) free-flow propagation of the plasma plume

ionization efficiency and to avoid jet quenching due to the higher concentration of  $O_2$  molecules delivered.

### 3 | CHARACTERIZATION OF THE DEPOSITED FILMS

#### 3.1 | Fourier transform infrared measurements

Fourier transform infrared (FTIR) measurements were performed on all the samples by means of an Agilent Cary 660 FTIR spectrometer in attenuated total reflectance (ATR) mode equipped with a monolithic diamond crystal and with the beam set at  $45^\circ$ , performing 32 scans with a scan resolution of  $4\text{ cm}^{-1}$ . A baseline correction was performed for each spectrum after the data acquisition. The spectra were normalized to one of the characteristic peaks of the PE substrate at  $\sim 2,913\text{ cm}^{-1}$ , corresponding to the stretching band of  $CH_2$  given by the substrate material only.

#### 3.2 | Water contact angle measurements

Static contact angle measurements were performed by means of a drop shape analyzer (DSA30; KRUSS): a distilled water drop ( $2\ \mu\text{l}$ ) was deposited on the sample substrate and the contact angle was measured using the Young–Laplace method.

#### 3.3 | Atomic force microscope measurement

The atomic force microscopy (AFM) analysis was performed with an Innova microscope (Bruker, Santa Barbara) and images were acquired in the air in AC mode at scan rates between 0.5 and 1 Hz. Semi-contact silicon cantilevers (RTESP; Bruker) with a spring constant of  $40\text{ Nm}^{-1}$  were employed. The surface topography of coatings was acquired by maintaining the first resonance amplitude of the tip constant. Images were processed with the manual tilt correction of the software SPIP (ImageMet).

#### 3.4 | Standard error of mean analysis

The coating morphology was investigated by means of the standard error of mean (Phenom G2 ProX), applying an accelerating voltage of 10 kV on sample sputters coated with gold. The energy dispersive X-ray analysis was performed on a different single area of the samples and the spectra obtained were analyzed using the Phenom ProSuite and Elemental Identification software packages.

#### 3.5 | Aging test in phosphate-buffered saline

Statically deposited films were dipped into 80 ml of the phosphate-buffered saline (PBS) solution at room

temperature to evaluate the water stability of the coatings. After 24 hr of immersion, samples were dried with compressed air and the FTIR spectra acquired were compared to those obtained before the stability test.

## 4 | RESULTS AND DISCUSSION

### 4.1 | Static deposition

#### 4.1.1 | FTIR characterization of statically deposited coatings

The ATR-FTIR spectra of ppHMDSO films at different oxygen contents are presented in Figure 2. The characteristic peaks of HMDSO, including the Si-O-Si asymmetric stretching mode, transversal optical mode 3 (TO3), between 1,000 and 1,150  $\text{cm}^{-1}$  due to the in-phase stretching vibration of oxygen atoms moving back and forth along the bound axis with a silicon atom, and the TO4 between 1,150 and 1,200  $\text{cm}^{-1}$ , responsible for the out-of-phase stretching of the oxygen atoms with respect to the Si atoms and appearing with the formation of glassy-like films containing defects (e.g., porosity, contamination, nonstoichiometry), Si-CH<sub>3</sub> symmetric deformation vibration mode (1,260  $\text{cm}^{-1}$ ), adsorbed water (3,000–3,600  $\text{cm}^{-1}$ ), the CH<sub>3</sub> rocking in Si-(CH<sub>3</sub>)<sub>2</sub> or/and TO of Si-O-Si at 800  $\text{cm}^{-1}$ , the Si-OH band at 925  $\text{cm}^{-1}$ , the C-H<sub>3</sub> at 2,965  $\text{cm}^{-1}$ , as well as the peaks due to the CH<sub>2</sub> present in the PE substrate at 720, 1,470, 2,850, and 2,915  $\text{cm}^{-1}$ , are recognized in the spectra.

As HMDSO contains six methyl groups, the initial coating deposited without oxygen is expected to show a strong organic character. However, the fragmentation of Si-CH<sub>3</sub> bonds and the removal of methyl groups with the introduction of oxygen result in coatings with an inorganic character.<sup>[30]</sup> This shift of organic to inorganic character makes the comparison and quantification of FTIR peaks more complicated, as similar chemical bonds are present in both kinds of coatings with very different conformation and constraints. Therefore, the evolution of peak intensity is not proportional to the thickness when comparing organic-like coatings and inorganic-like coatings. It should also be noted that no significant variation of thickness is expected, except for the condition without O<sub>2</sub>. This is because the HMDSO quantity is constant and there has been an excess of O<sub>2</sub>, compared with HMDSO, since the first addition of the lowest quantity of O<sub>2</sub>. Only the polymer cluster size in the gas phase varies with the O<sub>2</sub> increase but the total quantity of matter deposited is expected to be quite constant. This hypothesis is confirmed on the spectra not normalized to the peaks related to the substrate, where the intensity of the peaks is quite similar, irrespective of the deposition conditions.

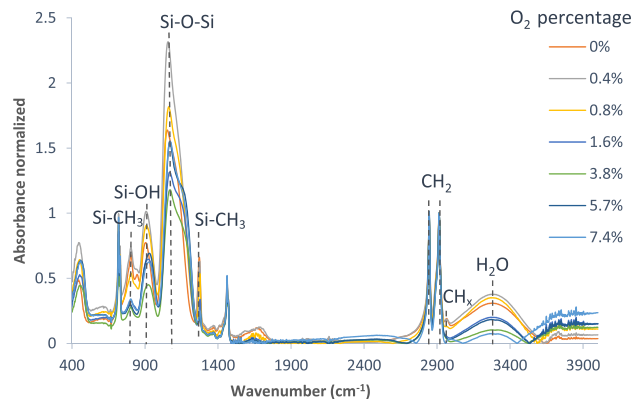


**FIGURE 2** Normalized Fourier transform infrared spectra for static deposition of hexamethyldisiloxane films with increasing O<sub>2</sub> content

The FTIR spectra show that all peaks are decreasing with the transition from organic to inorganic character, except the right shoulder of Si-O-Si peak (1,150–1,200  $\text{cm}^{-1}$ ), corresponding to TO4 (Figure 3). The decrease of peaks' intensities is sharp and occurring at a specific oxygen-added quantity around 1.5%, where the transition between polymer-like and glassy-like coatings occurs.

The decrease of the area of the peaks linked to the organic bonds (Si-CH<sub>3</sub>, CH<sub>3</sub>) was expected. The decrease of the other peaks (TO1, TO2, TO3, Si-OH, H<sub>2</sub>O) is not trivial at a constant amount of the matter. It can be explained by much more constrained bonds in the “glassy-like structure,” compared with the “polymer-like structure” for TO1 (transversal optical rocking), TO2 (transversal optical bending), and TO3 (transversal optical stretching) peaks. For the Si-OH and H<sub>2</sub>O, the decrease can be explained by a decrease of silanol groups replaced by a full Si-O-Si network when oxygen admixture increases. A similar trend can be observed in a heat treatment of silica coatings elaborated at low temperature in the presence of humidity.

The increase in TO4 peak can be mainly explained by the formation of a glassy-like coatings containing a significant amount of defects (pores, nonstoichiometry, or contaminants such as C or N).<sup>[31]</sup>

By increasing the oxygen concentration in plasma, the Si-O-Si peak gets wider due to the appearance and then widening of the component corresponding to TO4 optical mode, suggesting a shift toward a silica-like polymer with an increasing amount of defects.

Also, to evaluate the quantity of defects in glassy-like coatings, the widening of the Si-O-Si peaks can be used. As can be seen in the plot (Figure 3), there is a constant increase in the quantity of defects in the silica coatings from 80 ml/min (1.6%).

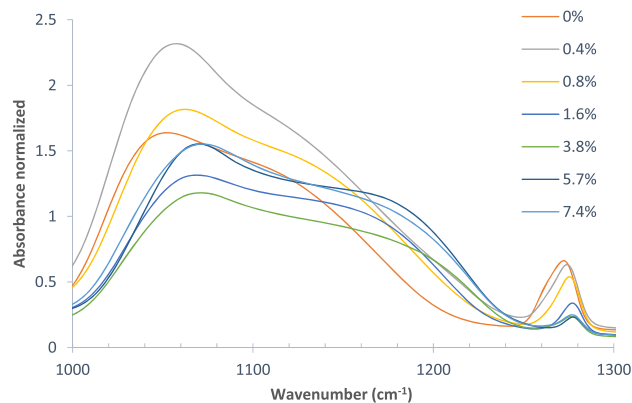


**FIGURE 3** Magnified Fourier transform infrared spectra of the statically deposited coatings from 1,000 to 1,300  $\text{cm}^{-1}$

Monitoring the variation in the intensity of the band attributed to  $\text{Si-CH}_3$  at 1,270–1,275  $\text{cm}^{-1}$ , representing the organic character of the coating can help interpret the evolution of the thin film with the  $\text{O}_2$  increase (Figure 4).

Comparing the moderate intensity of the second peak for the  $\text{Si-CH}_3$  band of plasma coatings with the intense peak for polydimethylsiloxane (PDMS) from the literature,<sup>[32]</sup> it can be concluded that the plasma coatings always present a higher inorganic character than intrinsic PDMS. This can be explained by the presence of oxygen in the environment, even without introducing it into the plasma gas.

#### 4.1.2 | Morphology of the statically deposited coatings

##### Scanning electron microscopy analysis

In Figure 5, scanning electron microscopy (SEM) images show an increase in roughness with the increase in  $\text{O}_2$  content in the plasma gas. As expected, the coatings become fragile (i.e., cracks appeared) when they present a high inorganic character. These observations from SEM analysis were also confirmed later during the AFM analysis. The samples presenting a high organic character show soft and adhesive properties that cause contaminations on the AFM tip, making characterization difficult (Figure 6a,b). However, in samples with a higher inorganic character, presenting a denser structure, this effect was not observed (Figure 6c–g).

##### Surface roughness characterization of the statically deposited coatings

As can be seen in the images for roughness analysis acquired by AFM for static depositions (see Figure 6), starting from the first image on the left (which is related to zero  $\text{O}_2$  content) to the image on the right (for

maximum oxygen content applied), the particle size and roughness increase following a logarithmic trend. We assume that these increases in roughness and particle size, which are correlated, are due to the increasing fragmentation of the precursor molecules by reactive oxygen species and the further polymer cluster aggregation in the gas phase favored by the higher density of reactive species.<sup>[33]</sup> These increasingly bigger aggregates are deposited on the surface, followed by coalescence, causing a higher surface roughness with  $\text{O}_2$  content. After a critical concentration of  $\text{O}_2$  (around 5%) is reached with a maximum root mean square (RMS) roughness of 30 nm, no more fragmentation of the precursor is possible, and the grain size of the depositing polymer clusters and roughness become constant (Figure 7). This plateau can be explained by an equilibrium between the growth/agglomeration of the polymer cluster and its etching in the gas phase. It is also shown that the roughness factor, which is defined by the ratio between the actual area and the projected surface area, is always below 1.3 over the whole range of oxygen content in the discharge.

##### WCA characterization of the statically deposited coatings

It has been reported that two parameters, in particular, define the wettability of organosilicon surfaces, the surface hydrocarbon content, and the surface roughness or roughness factor.<sup>[34]</sup> However, several studies have proven the effect of  $\text{O}_2$  gas introduction on surface hydrophilicity during plasma-assisted deposition of HMDSO; in fact, the presence of oxygen molecules in the gas phase enhances the in-flight reaction rate, increasing monomer fragmentation and reducing the organic character of deposited coatings.<sup>[35,36]</sup> Figure 8 shows the variation trend of water contact angle (WCA) values against oxygen

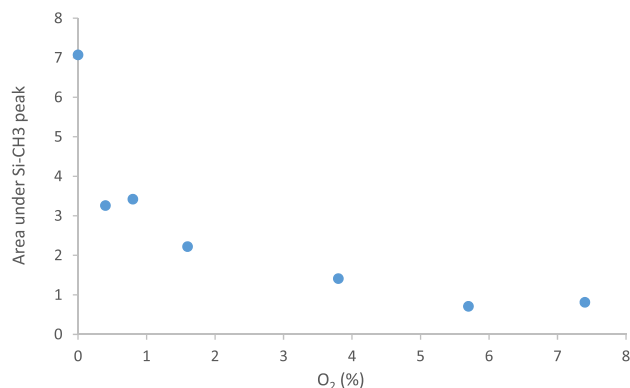


**FIGURE 4** The plot represents integration of the peaks attributed to the  $\text{Si-CH}_3$  band at around 1,270  $\text{cm}^{-1}$  recorded for statically deposited coating versus oxygen percentage

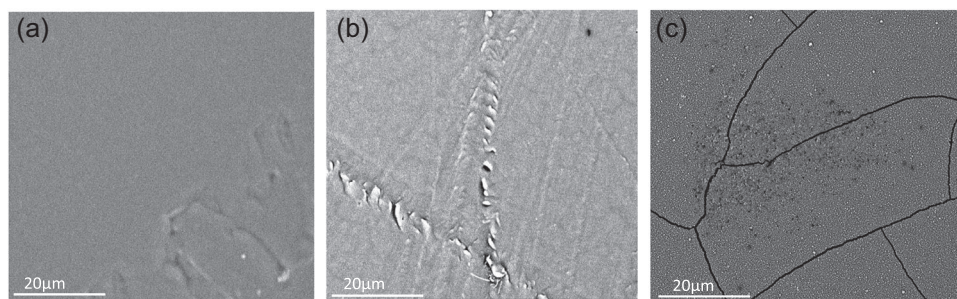


**FIGURE 5** Scanning electron microscopy images of statically deposited coatings: (a) untreated polyethylene, (b) the first deposition condition with 0% O<sub>2</sub>, (c) the last deposition condition with 7.4% O<sub>2</sub>

concentration in the plasma discharge region. The experimental data outline that a gradual increase in the oxygen flow rate in the Ar flow leads to an exponential decay of WCA value. This decay of WCA can be related to the exponential decay of the organic character until 200 ml/min (3.8%) of O<sub>2</sub>, as shown in Figure 4. This means that the variation of WCA is mainly related to the varying chemical composition of the coatings (including exponential decay). Then, a possible change in the nature of the silica surface leads to an additional decrease of WCA until 0°. The maximum WCA for 0% O<sub>2</sub> was around 97°, which is in agreement with the ~100° value observed for conventional (no effect of roughness) bulk PDMS.<sup>[37]</sup> At the opposite end of the gradient where the silica-like coating is present, the WCA was shown to be close to 0°, that is, lower than the WCA expected on amorphous smooth silica surfaces (40–50°).<sup>[38]</sup> This superhydrophilic behavior cannot be explained by the roughness factor, which always remains below 1.3, as discussed in Reference [39]. Therefore, we assume that this unexpected superhydrophilic behavior is due to the silica film with a higher content of silanol hydrophilic groups, as shown on the FTIR spectra (Figure 2), with the peak appearing at 950 cm<sup>-1</sup>. This specific chemical state of plasma SiO<sub>2</sub> films can be reached due to the long plasma exposure in the most oxidant conditions. A hypothesis can be formulated: these extreme conditions favor the postdeposition reactions of the coating with the ambient moisture, due to microstructural defects generated by etching in the gas phase and on the film. Identically, the WCA of the coatings is always lower on the edge of the plasma coatings, because more reactive species or specific conditions are generated at the interface due to plasma or gas flow inhomogeneities, leading to more defective coatings prone to silanol formation in contact with air. In conclusion, it is shown that a wide range of WCAs can be achieved with the Corona jet by using a single precursor, HMDSO.

#### Aging test in PBS

The FTIR spectra for the stability test of the coatings with 0%, 0.4%, and 7.4% oxygen content are shown in Figure 9. Comparing the FTIR spectra obtained for each coating before and after immersion in PBS, and considering the organosilicon peaks (Si–O–Si and Si–CH<sub>3</sub>), it can be concluded that the coatings have a satisfactory stability in the PBS solution, irrespective of the organic/inorganic character, because the organosilicon peaks do not show significant variation after 24 hr of immersion in PBS. However, stability decreases slowly with the increase of the inorganic character, as shown with the variation of intensity in some peaks (at 900 or 3,400 cm<sup>-1</sup>). This result confirms the promising stability of the coatings in a physiological medium at neutral pH, indicating that the PDMS-like coating (without oxygen addition) is already well cross-linked.

## 4.2 | Dynamic deposition

### 4.2.1 | FTIR characterization of the gradient coating

FTIR measurements were performed in each area related to the deposition condition along the gradient line and in the middle of the coating (see Figures 10 and 11). The same analysis process for statically deposited coatings was applied to the gradient lines generated in the dynamic mode and identical peaks were used to interpret the chemistry of the coating. As expected, a similar trend was observed for the structure/defect evolution and organic character of the gradient coatings, as can be seen in Figure 12. An increase in the structural defects and a decrease in the organic features of the gradient were observed toward the end of the gradient where the coating demonstrated high inorganic features. The plots for dynamic deposition demonstrated similar trends but

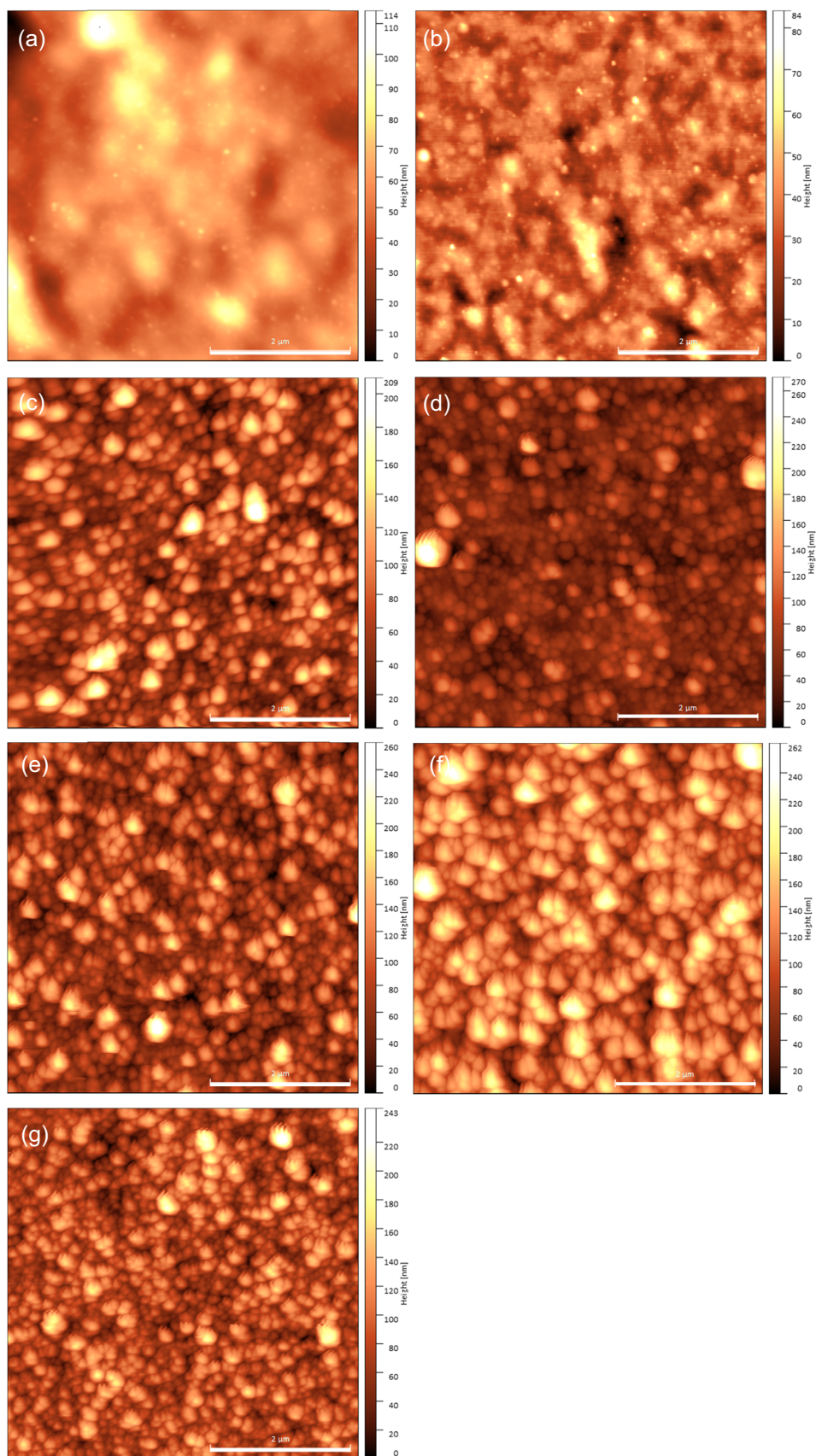


**FIGURE 6** Atomic force microscopy tapping mode images of the organosilicon statically deposited spots with increasing  $O_2$  content over the polyethylene substrate. The measurements were made at the center of the coating. (a) 0%  $O_2$ , (b) 0.4%  $O_2$ , (c) 0.8%  $O_2$ , (d) 1.6%  $O_2$ , (e) 3.8%  $O_2$ , (f) 5.7%  $O_2$ , (g) 7.4%  $O_2$ , and (e) the images were obtained on a  $5 \mu\text{m} \times 5 \mu\text{m}$  scale with a 0.7-Hz scan rate. Scale bars show  $2 \mu\text{m}$  length on the surface



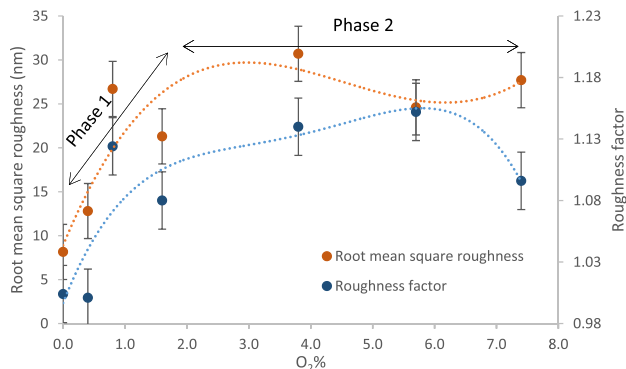


**FIGURE 7** Roughness evolution for statically deposited plasma coatings versus an increase in oxygen concentration in the plasma gas (percentage)

with more gradual changes from organic to inorganic features, compared with static deposition; these are probably a consequence of the noninstantaneous variation (a few ms) provided by the mass flow controller, which instead produced a gradual transition from the O<sub>2</sub> flow set in a certain condition, resulting in a gradual variation of the coating characteristics. The static deposits, instead, present sharp transitions between each investigated case, as these cases are deposited separately and stable O<sub>2</sub> gas flow was reached before starting the deposition process. In addition, there is an increase in the structural defects' concentration of the gradient coating versus oxygen flow rate with a more gradual slope, compared with the static condition, which maybe also due to the fact that the concentration of oxygen is lower close to the substrate due to the jet movement, which is adding nitrogen from air, and the saturation point is not easily detectable, unlike the significant saturation state observed for the static condition.

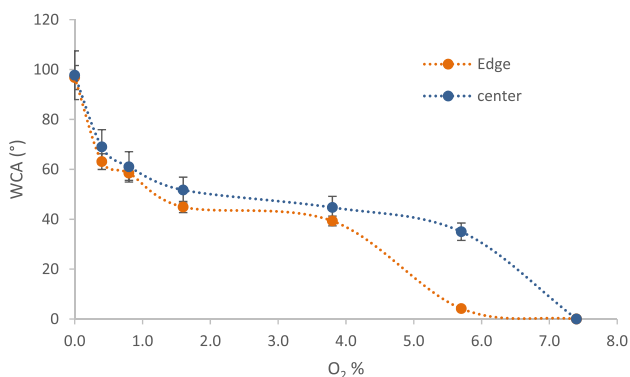


**FIGURE 8** Water contact angles (WCAs) measured for the statically deposited coatings at the center and edge of the coatings versus O<sub>2</sub> content in the gas phase

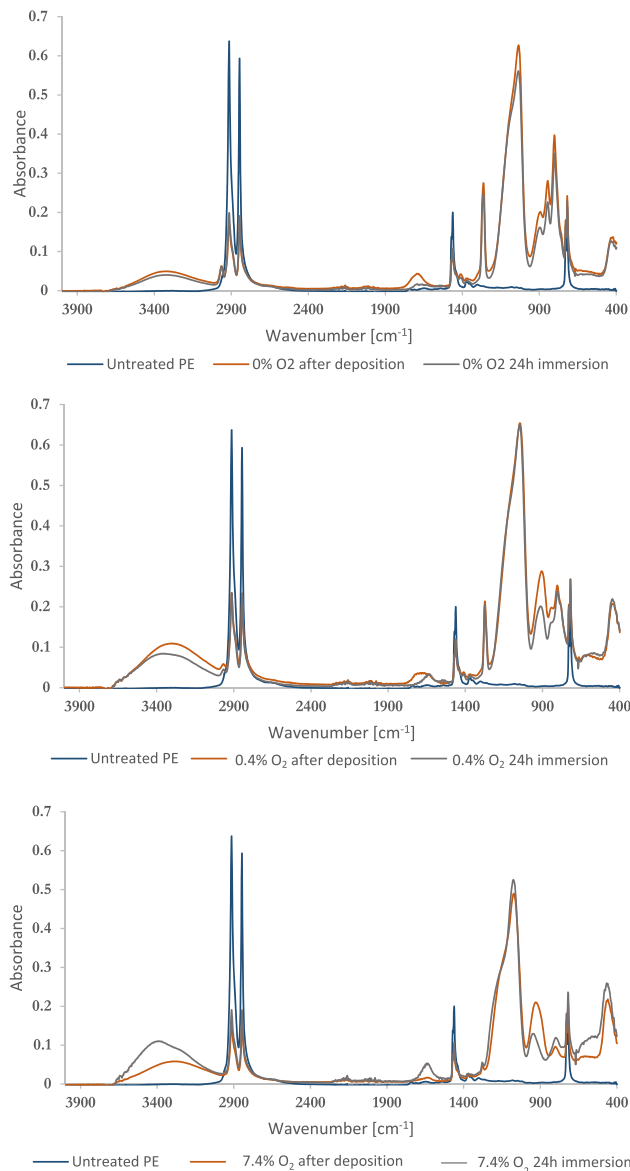


**FIGURE 9** Fourier transform infrared characterization of the three statically deposited coatings immersed in phosphate-buffered saline as a stability test. PE, polyethylene

#### 4.2.2 | Surface roughness characterization of the gradient coating

The gradient line generated, starting from 0% and ending at 7.4% O<sub>2</sub>, was characterized at different positions along the gradient line by AFM in the tapping mode (see Figure 13). It can be observed that the initial rounded and flat protuberances corresponding to the deposition of the precursor in the absence of oxygen gradually coalesce after introducing oxygen and evolve into bigger protuberances (typical of polymer-based coatings), as already observed for the static deposition mode. By introducing O<sub>2</sub> (Figure 13c) when the precursor is partially decomposed (Phase 1), better-defined grains start to appear and,

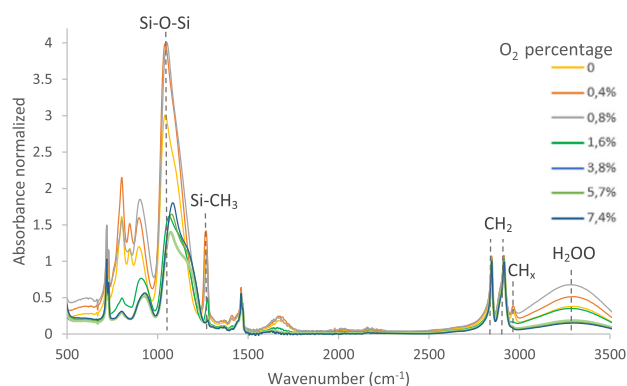


**FIGURE 10** Normalized Fourier transform infrared spectra for gradient line of hexamethyldisiloxane film at the center of the coating with increasing  $O_2$  content (0–7.4%  $O_2$ ) after baseline correction

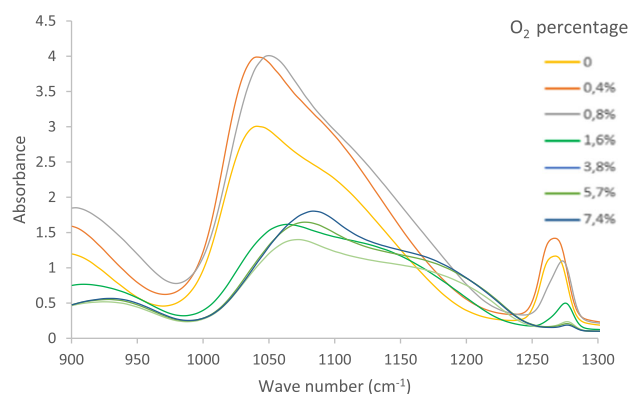


**FIGURE 11** Magnified Fourier transform infrared spectra of the gradient coating at  $950\text{--}1,300\text{ cm}^{-1}$

by further increasing the oxygen rate, bigger well-defined grains are formed as a result of the full decomposition of the precursor, contributing to the increase of the surface roughness to the maximum (Phase 2). This increase is

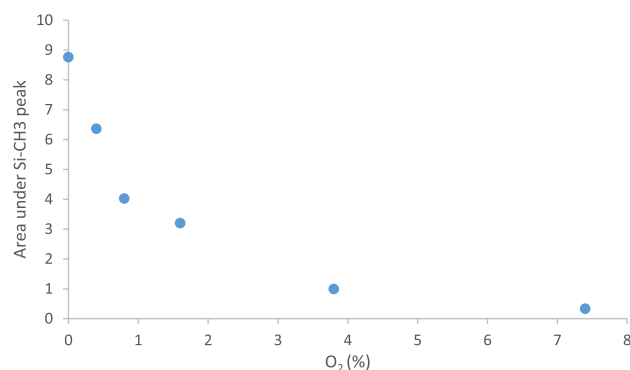


**FIGURE 12** The integration of the peaks attributed to the  $Si-CH_3$  band at around  $1,270\text{ cm}^{-1}$  along the gradient coating versus oxygen percentage is presented

evident when looking at the variation of the height of the randomly selected grains in the cross-section texture profiles. (Figure 13, right panel). Here again, the transition from flat protuberance to well-defined grains is slower in the dynamic deposition mode. For the higher oxygen contents (Phase 3), the decrease in surface structure height (Figure 13g) can be explained as an etching effect due to the production of an excess of oxygen radicals when the precursor is already fully fragmented with oxygen, as already observed in the static deposition mode.

The image analysis for the several points along the gradient coating demonstrated a roughness variation in the range of 10–70 nm (see Figure 14). Compared with the static deposition mode, there is a more gradual increase of roughness and a higher roughness maximum is reached. Another difference observed is also a higher decrease of roughness after reaching this maximum roughness. The evolution of roughness can be broken down into three phases. In Phase 1, the precursor continues decomposing and the clusters of polymers formed in the gas phase become bigger. In Phase 2, the precursor is becoming fully decomposed and an equilibrium between the polymer cluster growth and etching is reached in the gas phase, leading to maximum cluster size and roughness. When the etching rate of polymer clusters in the gas phase is higher than the growth rate, there is a decrease in the average cluster size in the gas phase, followed by a decrease of the roughness of the coating. An additional etching on the grains, when deposited on the surface, is also possible for the highest contents of  $O_2$ , but it is supposed to be much lower than the etching in the gas phase, where conditions are harsher and clusters easier to etch (Phase 3), as discussed previously. A different mixture of reactive species due to the movement of the jet mixing the ambient air with the plasma could explain why bigger polymer clusters are formed and why a significant etching at a critical amount of oxygen admixture is observed for dynamic deposition, compared with static deposition.

Moreover, the previously mentioned delay in the response time for dynamic deposition can explain the slower shift of the coating from its organic character with small protuberances to an inorganic character with bigger grains.

### 4.2.3 | WCA characterization of the gradient coating

WCA values obtained for gradient plasma film at the center of the coatings demonstrate a trend similar to that of values measured for statically deposited coating conditions, confirming generally the successful generation of wettability gradients along the coating. Here again, the evolution can

be broken down into three phases. Initially, there is an abrupt decrease of up to 0.8% oxygen gas introduction, mainly due to the fast decrease of  $\text{CH}_x$  content in the coating (Figure 15). In the second phase, a plateau is reached for intermediate  $\text{O}_2$  flow rates in the range of 0.8–3.8% gas, as observed for static deposition. This plateau can be explained by a coating already containing a maximum of Si–O–Si bonds and a minimum of  $\text{CH}_x$  in the coating (full decomposition of the precursor at this stage

with  $\text{CH}_x$  evacuated in the atmosphere). In Phase 3, a sharp decrease of WCA after 3.8% oxygen introduction is observed. This decrease of WCA is more important for the static deposition mode with a minimum WCA close to zero (superhydrophilic). As this higher decrease of WCA cannot be explained by a significant change in roughness or roughness factor (Figure 14), we hypothesized that it is mainly due to a change in the chemical composition/microstructural defect in the coatings, leading to a higher

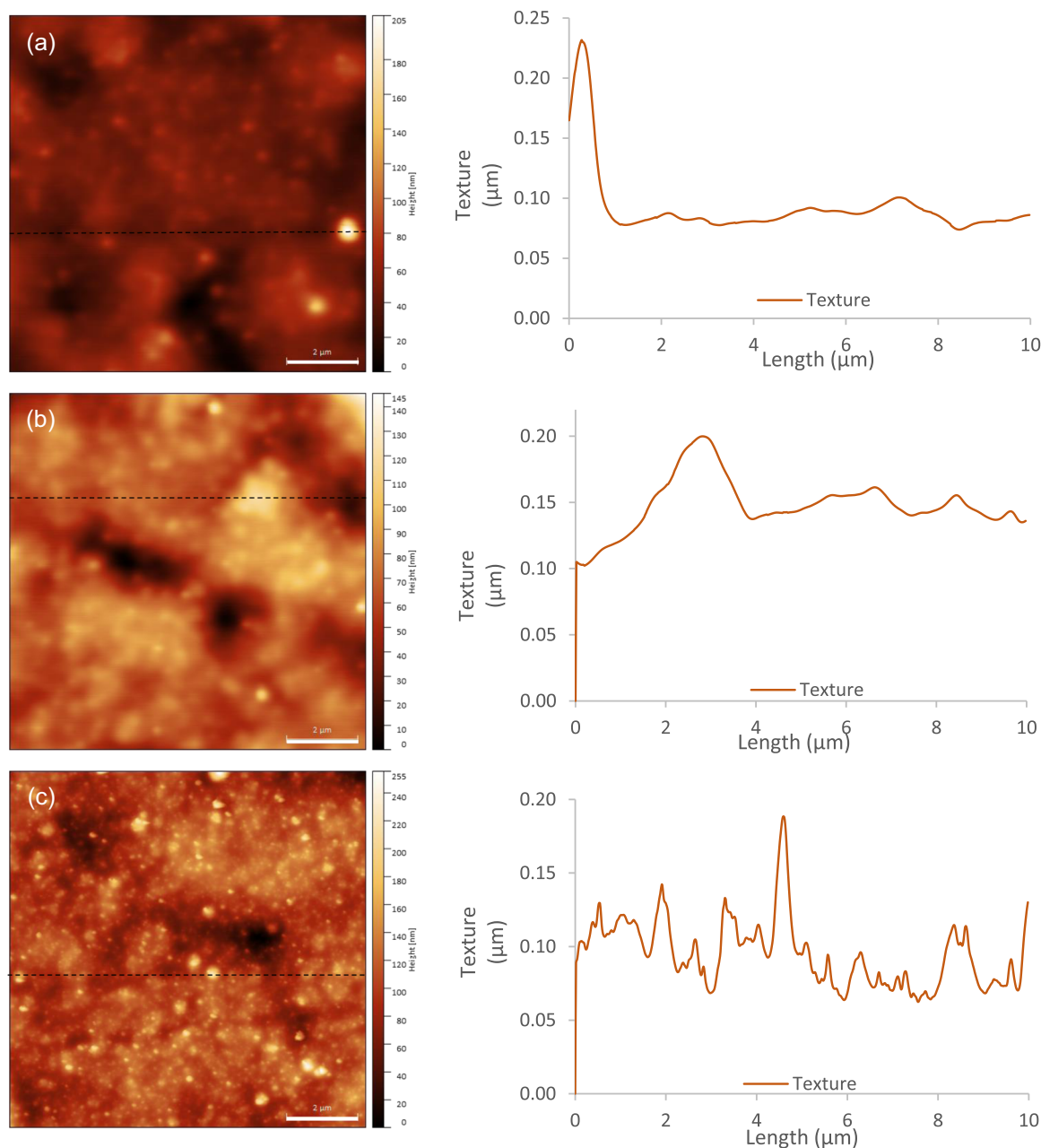


**FIGURE 13** Atomic force microscopy tapping mode images of the organosilicon gradient with increasing  $\text{O}_2$  values over the polyethylene surface (on the left) and height profile of the randomly selected surface section (on the right). (a) Position 0 mm from the start of the line with 0%  $\text{O}_2$ , (b) 10 mm from the start with %  $\text{O}_2$ , (c) 20 mm from start with 0.4%  $\text{O}_2$ , (d) 52 mm from start with 0.8%  $\text{O}_2$ , (e) 67 mm from start and 1.6%  $\text{O}_2$ , (f) 97 mm from start with 5.7%  $\text{O}_2$ , and (g) 125 mm from start with 7.4%  $\text{O}_2$ . Scale bars show 2- $\mu\text{m}$  length on the surface

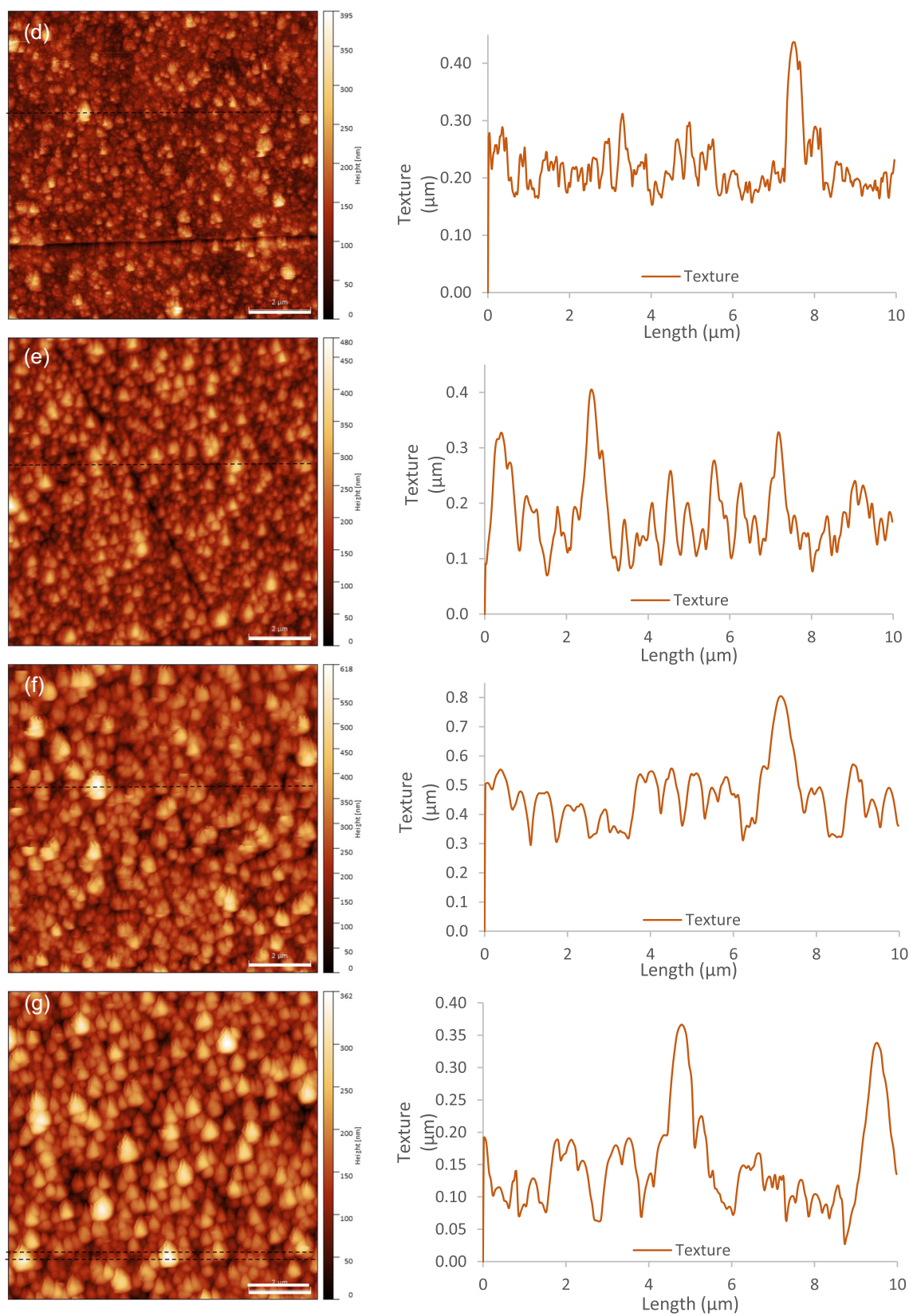
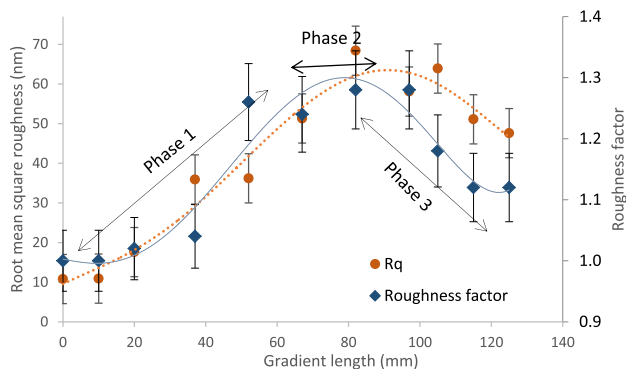


FIGURE 13 (Continued)



**FIGURE 14** Plots depict the roughness evolution along the gradient coating with 0–7.4% oxygen introduction with total 135-mm length versus distance from the starting point of the gradient coating. Atomic force microscopy measurements were made twice on each point and the scanned area was  $10\ \mu\text{m}$  in the central region of the deposited line

content of hydrophilic groups in the coatings, as shown on the FTIR spectra (e.g., silanol, OH). The decrease of WCA is less important for the dynamic deposition mode due to the mixing of ambient air and plasma jet, leading to a lower density of the reactive oxygen species (dilution effect).

## 5 | CONCLUSION

In this study, we obtained a fast and economic way of optimizing surfaces (combinatorial approach) by means of surface gradients deposited with an atmospheric plasma jet for developing biosensors or devices, which will be in contact with biological or complex media. It was observed that by continuously increasing the oxygen content in the gas phase during the deposition of polymers, the morphology, chemistry, and wettability of the surface gradually

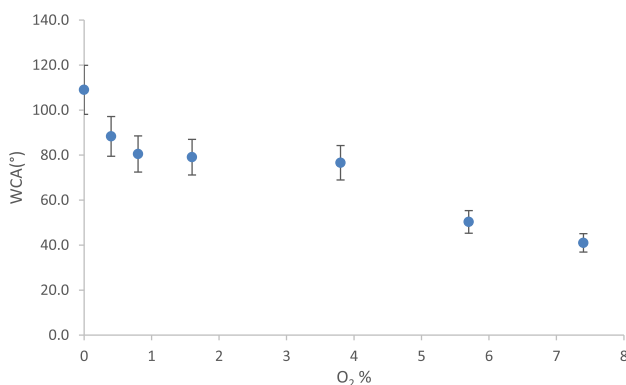


**FIGURE 15** Water contact angles (WCAs) measured for the gradient line at the center of the plasma film coating as a function of O<sub>2</sub> content in the gas phase

changed, offering more inorganic and hydrophilic surfaces with increased roughness at an intermediate concentration of oxygen, which can aid biomolecule, that is, cell adhesion and proliferation. These surface changes are thought to be mainly due to a change of polymer cluster size and nature in the gas phase, just before deposition on the polymer substrate. The differences observed for the dynamic deposition mode are due to a more linear variation of deposition conditions and a higher content and slightly different nature of reactive species due to the mixing of ambient air and plasma gas with a cluster inside, owing to the movement of the jet. The good stability of the coatings in a physiological liquid (PBS) indicated possible applications of the gradient surface for biosensing, even if a slight stability decrease was observed for more inorganic regions. Meanwhile, surface gradients are also suitable for direct application in chemotaxis studies. PE substrate was selected as a model of a sensitive substrate, and deposition with atmospheric plasma did not show any degradation of the polymer substrate in selected deposition conditions, suggesting that this approach is suitable for depositing HMDSO-based coating gradients on heat-sensitive materials. Plasma gradient was obtained on a range of several cm and width of 2 cm, with roughness values varying between 10 and 70 nm and wettability varying between  $110^\circ$  and  $40^\circ$  WCA, and with a jet moving speed of 15 mm/min with 6 min of deposition time per full gradient coatings.

These results reveal the possibility of achieving a gradual variation of the chemistry and roughness by dynamic deposition. Meanwhile, dynamic deposition provided a higher amplitude of roughness and WCA as compared with static deposition ( $70$  vs.  $35$  nm;  $110^\circ$  vs.  $80^\circ$ ).

As an ideal gradient is expected to show a complete linearity between the varying property and the length of the gradient, with a high amplitude for the variable, the next step is to improve linearity and expand amplitude in variables. Lateral resolution as a limitation for plasma jets is also an aspect that will be addressed in the near future as instrumentation advances.

## ORCID

Hediyeh Malekzad  <http://orcid.org/0000-0002-8924-9747>

Federica Barletta  <http://orcid.org/0000-0001-8920-9203>

## REFERENCES

- [1] R. Förch, A. N. Chifen, A. Bousquet, H. L. Khor, M. Jungblut, L. Q. Chu, Z. Zhang, I. Osey-Mensah, E. K. Sinner, W. Knoll, *Chem. Vap. Deposition* **2007**, *13*, 280.
- [2] O. Bazaka, K. Bazaka, in *Biomaterials and Medical Device-Associated Infections*, Elsevier, Oxford, UK 2015, Ch.6.
- [3] M. S. Kim, G. Khang, H. B. Lee, *Prog. Polym. Sci.* **2008**, *33*, 138.
- [4] I. Caelen, H. Gao, H. Sigrist, *Langmuir* **2002**, *18*, 2463.

- [5] J. Yang, F. R. Rose, N. Gadegaard, M. R. Alexander, *Adv. Mater.* **2009**, *21*, 300.
- [6] V. Sourjik, N. S. Wingreen, *Curr. Opin. Cell Biol.* **2012**, *24*, 262.
- [7] S.-J. Wang, W. Saadi, F. Lin, C. Minh-Canh Nguyen, N. Li Jeon, *Exp. Cell Res.* **2004**, *300*, 180.
- [8] P. Lee, C. S. Chen, T. Gaige, P. J. Hung, *Nat. Methods* **2015**, *12*, vii.
- [9] M. Vandebossche, M.-I. B. Garcia, U. Schütz, P. Rupper, M. Amberg, D. Hegemann, *Plasma Chem. Plasma Process.* **2016**, *36*, 667.
- [10] M. M. Hossain, D. Hegemann, G. Fortunato, A. S. Herrmann, M. Heuberger, *Plasma Processes Polym.* **2007**, *4*, 471.
- [11] H. J. Lee, A. C. Jamison, T. R. Lee, *Langmuir* **2015**, *31*, 2136.
- [12] K. L. Parry, A. Shard, R. Short, R. White, J. Whittle, A. Wright, *Surf. Interface Anal.* **2006**, *38*, 1497.
- [13] J. D. Whittle, D. Barton, M. R. Alexander, R. D. Short, *Chem. Commun.* **2003**, *14*, 1766.
- [14] F. J. Harding, L. R. Clements, R. D. Short, H. Thissen, N. H. Voelcker, *Acta Biomater.* **2012**, *8*, 1739.
- [15] D. J. Menzies, B. Cowie, C. Fong, J. S. Forsythe, T. R. Gengenbach, K. M. McLean, L. Puskar, M. Textor, L. Thomsen, M. Tobin, B. W. Muir, *Langmuir* **2010**, *26*, 13987.
- [16] A. Mierczynska, A. Michelmor, A. Tripathi, R. V. Goreham, R. Sedev, K. Vasilev, *Soft Matter* **2012**, *8*, 8399.
- [17] M. Yildirim, U. Hasanreisoglu, N. Hasirci, N. Sultan, *J. Oral Rehabil.* **2005**, *32*, 518.
- [18] H. T. Spijker, R. Bos, H. J. Busscher, T. G. van Kooten, W. van Oeveren, *Biomaterials* **2002**, *23*, 757.
- [19] J. H. Lee, J. W. Lee, G. Khang, H. B. Lee, *Biomaterials* **1997**, *18*, 351.
- [20] W. G. Pitt, *J. Colloid Interface Sci.* **1989**, *133*, 223.
- [21] C. G. Gölander, W. G. Pitt, *Biomaterials* **1990**, *11*, 32.
- [22] H.-B. Lee, M.-S. Kim, Y.-H. Cho, G.-S. Khang, J.-H. Lee, *Polymer* **2005**, *29*, 423.
- [23] J. Philipp, A. K. Czerny, C. P. Klages, *Plasma Processes Polym.* **2016**, *13*, 509.
- [24] D. E. Robinson, D. J. Buttle, J. D. Whittle, K. L. Parry, R. D. Short, D. A. Steele, *Plasma Processes Polym.* **2010**, *7*, 102.
- [25] I. Hopp, M. N. MacGregor, K. Doherty, R. M. Visalakshan, K. Vasilev, R. L. Williams, P. Murray, *ACS Biomater. Sci. Eng.* **2019**, *5*, 2834.
- [26] X. Liu, S. Shi, Q. Feng, A. Bachhuka, W. He, Q. Huang, R. Zhang, X. Yang, K. Vasilev, *ACS Appl. Mater. Interfaces* **2015**, *7*, 18473.
- [27] M. Affolter, K. Basler, *Nat. Rev. Genet.* **2007**, *8*, 663.
- [28] S. Kotula, M. Lüdemann, J. Philipp, M. Thomas, C.-P. Klages, *Plasma Processes Polym.* **2017**, *14*, 1600137.
- [29] F. Barletta, A. Liguori, C. Leys, V. Colombo, M. Gherardi, A. Nikiforov, *Mater. Lett.* **2018**, *214*, 76.
- [30] R. A. Siliprandi, S. Zanini, E. Grimoldi, F. S. Fumagalli, R. Barni, C. Riccardi, *Plasma Chem. Plasma Process.* **2011**, *31*, 353.
- [31] S. Ponton, F. Dhainaut, H. Vergnes, D. Samelot, D. Sadowski, V. Rouessac, H. Lecoq, T. Sauvage, B. Caussat, C. Vahlas, *J. Non-Cryst. Solids* **2019**, *515*, 34.
- [32] K. R. Aguiar, V. G. Santos, M. N. Eberlin, K. Rischka, M. Noeske, G. Tremiliosi-Filho, U. P. Rodrigues-Filho, *RSC Adv.* **2014**, *4*, 24334.
- [33] A. Kilicaslan, O. Levasseur, V. Roy-Garofano, J. Profili, M. Moisan, C. Côté, A. Sarkissian, L. Stafford, *J. Appl. Phys.* **2014**, *115*, 113301.
- [34] I. Nouicer, S. Sahli, M. Kihel, Z. Ziari, A. Bellel, P. Raynaud, *Int. J. Nanotechnol.* **2015**, *12*, 597.
- [35] K. N. Pandiyaraj, A. Arun Kumar, M. C. Ramkumar, S. U. Kumar, P. Gopinath, P. Cools, N. De Geyter, R. Morent, M. Bah, S. I. Shah, P. G. Su, R. R. Deshmukh, *Vacuum* **2017**, *143*, 412.
- [36] V. Purohit, E. Mielczarski, J. A. Mielczarski, L. Akesso, *Mater. Chem. Phys.* **2013**, *141*, 602.
- [37] D. Keskin, T. Mokabbar, Y. Pei, P. Van Rijn, *Polymers* **2018**, *10*, 534.
- [38] M. Śliwińska-Bartkowiak, A. Sterczyńska, Y. Long, K. E. Gubbins, *Mol. Phys.* **2014**, *112*, 2365.
- [39] J. Drelich, E. Chibowski, D. D. Meng, K. Terpilowski, *Soft Matter* **2011**, *7*, 9804.

**How to cite this article:** Malekzad H, Galligani T, Barletta F, Gherardi M, Colombo V, Duday D. Single-step deposition of hexamethyldisiloxane surface gradient coatings with a high amplitude of water contact angles over a polyethylene foil. *Plasma Process Polym.* 2021;18:e2000044. <https://doi.org/10.1002/ppap.202000044>